Journal of Photochemistry & Photobiology, A: Chemistry 457 (2024) 115881

Contents lists available at ScienceDirect

Journal of Photochemistry & Photobiology, A: Chemistry

journal homepage: www.elsevier.com/locate/jphotochem

Precision detection of cyanide, fluoride, and hydroxide ions using a new tetraseleno-BODIPY fluorescent sensor

Beatriz S. Cugnasca [a,b], Frederico Duarte [b], João L. Petrarca de Albuquerque [a], Hugo M. Santos [b,c], José Luis Capelo-Martínez [b,c], Carlos Lodeiro [b,c,*], Alcindo A. Dos Santos [a,**]

[a] Institute of Chemistry, Department of Fundamental Chemistry, University of São Paulo, 05508-000 São Paulo, SP, Brazil
[b] BIOSCOPE Research Group, LAQV-REQUIMTE, Department of Chemistry, NOVA-FCT, NOVA University Lisbon, 2829-516 Caparica, Portugal
[c] PROTEOMASS Scientific Society, 2825-466 Costa da Caparica, Portugal

ARTICLE INFO

Keywords:
BODIPY
Fluorescence probe
Selenium
Cyanide
Fluoride
Chemosensor

ABSTRACT

A new chemosensor based on Seleno-BODIPY **(4)** was designed and synthesized for the rapid and sensitive detection of CN^-, F^-, and OH^- ions in THF, exhibiting ultra-low detection limits of 26.26 nM, 43.05 nM, and 8.64 nM, respectively, through a turn-on fluorescent process. The seleno-funcionalization step was based on a novel methodology developed by our group, allowing direct functionalization of the BODIPY core. This procedure involves a quick reaction utilizing Ph_2Se_2 as a selenium source, BPO (benzoyl peroxide), and *p*-TSA (p-toluenesulfonic acid) in acetonitrile, enabling the production of the corresponding chalcogenated BODIPYs containing one to four selenium groups, demonstrating its versatility. The structure of BODIPY **4** was confirmed by HRMS, ^1H, ^{13}C, ^{77}Se NMR, and IR spectra, and its photophysical properties were also evaluated. BODIPY **4** was applied to detect CN^-, F^-, and OH^- ions in dual-mode detection (UV–Vis and fluorescence spectra), displaying a ratiometric response. The new probe exhibited a fast response time, visual color change from blue to fluorescent yellow, and high sensitivity and selectivity for these analytes over other selected anions. Mechanistic investigation through mass analysis revealed that the detection of these anions by BODIPY **4** occurs via an Aromatic Nucleophilic Substitution reaction with phenylselenide as the leaving group.

1. Introduction

In recent decades, the interest in developing new sensors for anion recognition has been a growing due to their fast response time, high selectivity, and sensitivity [1–3]. Among the various anions studied, fluoride (F^-) and cyanide (CN^-) are particularly important in environmental, clinical and biological process, and in industrial settings. CN^- is widely used in industrial processes, including the production of synthetic fibers, metal cleaning, and electroplating [2,4]. It can also be found in pigments and certain foods such as almonds, cassava, and soybeans [5–7]. Additionally, cyanide is used in analytical chemistry quantification methods. Due to its extreme toxicity, the World Health Organization (WHO) has established a maximum permissible level of 1.9 μM of CN^- in drinking water [8]. F^- is prevalent in everyday life, being used in dental care, osteoporosis treatment, and tooth decay prevention. It is commonly found in toothpaste and water samples. In industry, F^- is used in the manufacture of insecticides, analytical reagents, and surface cleaning agents [9,10]. However, excessive F^- can lead to kidney and gastric diseases when concentrations exceed 2.0 mg/L and fluorosis when above 4.0 mg/L [10,11]. Therefore, monitoring the concentration of F^- and CN^- in everyday goods samples is extremely important for public health.

In this context, numerous conventional methods for detecting and quantifying $CN^-$and F^- ions have been developed, including potentiometry, voltammetry, titration, electrochemistry, and others [12–15]. Although these techniques are effective, their use is often constrained by the need for expensive equipment, rigorous sample preparation, and the necessity of highly trained personnel. Therefore, fluorescent sensors present a compelling alternative [16–18]. They offer several advantages, such as experimental simplicity, real-time analysis, cost-effectiveness, and the capability to perform non-destructive sample analysis [7,19,20]. Consequently, a variety of sensors have been developed for

* Corresponding author at: BIOSCOPE Research Group, LAQV-REQUIMTE, Department of Chemistry, NOVA-FCT, NOVA University Lisbon, 2829-516 Caparica, Portugal.
** Corresponding author at: Institute of Chemistry, Department of Fundamental Chemistry, University of São Paulo, 05508-000 São Paulo, SP, Brazil.
E-mail addresses: cle@fct.unl.pt (C. Lodeiro), alcindo@iq.usp.br (A.A. Dos Santos).

https://doi.org/10.1016/j.jphotochem.2024.115881
Received 30 May 2024; Received in revised form 29 June 2024; Accepted 8 July 2024
Available online 9 July 2024

the detection of F^- and CN^-. Numerous sensors have been reported for the specific detection of F^- ions, as well as for CN^- ions. Moreover, several studies have described sensors capable of detecting both F^- and CN^- ions. These advancements highlight the potential of fluorescent sensors to surpass traditional methods, making them highly valuable in various applications [10,21,22].

Another anion that deserves attention is the hydroxide (OH^-). Caustic soda (NaOH) is involved in numerous industrial processes, including high-concentration alkaline baths for neutralization reactions, removal of acid gases, sodium salt production, electroplating, and wastewater treatment. As a result, NaOH is considered one of the most significantly manufactured industrial feedstocks worldwide [23,24]. Due to its corrosivity, the development of online monitors for detecting high concentrations of OH^- is limited [24,25]. While electrochemical sensors are commonly used to measure *p*H, they tend to produce significant experimental errors in extreme alkaline conditions (above pH 11) and reduce the durability of *p*H-meter materials [23,24,26]. Other methods for quantifying OH^- include flow injection analysis (FIA), near-infrared spectroscopy (NIRS), conductometry, and titrimetry [24,27]. Considering the need for practicality, quick response time, and real-time analysis, optical sensors offer a promising alternative to these challenges. Despite their potential, optical sensors have been underexplored for OH^- ion detection [28].

The insertion of chalcogenated groups into a chemosensor is a recently prominent and advantageous strategy [29], as these groups lead to fluorescence quenching [30] through mechanisms like Photoinduced Electron Transfer (PeT) and Internal Charge Transfer (ICT) [31]. This quenching often results in a non-fluorescent emission background, enabling chalcogenated sensors to function as on/off fluorescence sensors. In the presence of analytes that interact or react with the chalcogenated portion of BODIPY, a turn-on fluorescence process occurs, allowing the BODIPY to serve effectively as a sensor. Common post-functionalization strategies for BODIPY core with selenium-containing groups include reactions using Ph_2Se_2 and $NaBH_4$ or selenomorpholine requiring prior halogenation of the BODIPY nucleus [32,33], selenylation reactions of previously halogenated aldehydes often involving multiple steps followed by the synthesis of functionalized BODIPY [34,35], coupling reactions with palladium [36], reactions of BODIPY with benzoyl chloride previously functionalized from Ph_2Se_2 [37], and direct functionalization of the BODIPY core with PhSeCl without prior halogenation [38]. These methods generally necessitate previous core functionalization, such as halogenation, or the use of expensive transition metal catalysts before introducing the chalcogen atom. Therefore, direct and metal-free methods are highly desirable to simplify the functionalization of BODIPYs.

Herein, we report a novel multifunctional fluorescent sensor for the selective detection and quantification of F^-, CN^-, and OH^- ions in dual modes (colorimetric and fluorometric), featuring a ratiometric response, high sensitivity, fast response time, ultra-low detection limits, and high fluorescence quantum yield. The probe was synthesized via a one-step metal-free direct functionalization of the BODIPY core. To the best of our knowledge, this represents the first selenium-based BODIPY sensor specifically designed for cyanide detection.

2. Experimental

2.1. Spectrophotometric and spectrofluorimetric measurements

The fluorescence emission spectra were recorded on a HORIBA JOBIN YVON FluoroMax-4 Spectrofluorometer, the emission spectra for fluorescence quantum yield were obtained on a JASCO FP-8350, and the UV–vis spectra on a JASCO V-650 spectrophotometer (PROTEOMASS-BIOSCOPE Scientific Society Facility). A stock solution of the BODIPY was prepared in THF (ca. 10^{-3} mol/L) in a 1 mL volumetric flask for the titrations, kinetic studies and characterizations of **4**. The stock solutions of anions were prepared in Milli-Q water (0.1 mol/L). Study solutions were prepared by appropriate dilutions of the stock solutions in THF to the desired final concentration. When it was necessary, a correction for the absorbed light was conducted. Quartz cuvettes (3 mL) were used in all experiments. The experiments were all performed at 298 K.

The limit of detection (LOD) and limit of quantification (LOQ) were calculated through the equation (1) and (2), respectively, performing ten different analyses in the equipment:

$$LOD = \frac{3\sigma}{k} \quad (1)$$

$$LOQ = \frac{10\sigma}{k} \quad (2)$$

where σ is the standard deviation obtained for 10 blank measurements (BODIPY **4** solution without the presence of any analyte), and k is the angular coefficient of the linear correlation obtained through the signal (emission) and the concentration of the analyte desired.

2.2. Fluorescence quantum yield

The fluorescence quantum yield (Φ) of the compounds obtained were calculated through Equation (3).

$$\Phi_s = \Phi_r \left(\frac{A_r}{A_s}\right)\left(\frac{E_s}{E_r}\right)\left(\frac{n_s}{n_r}\right)^2 \quad (3)$$

Where Φ = fluorescence quantum yield, A = absorbance at excitation wavelength of solution, E = area under the emission curve, n = refractive index of the solvent. Subscripts "s" and "r" denotes sample and standard, respectively [39].

2.3. Synthetic procedures

a) Synthesis of aldehyde (**1**) (4-(2-(2-(2-hydroxyethoxy)ethoxy) ethoxy)benzaldehyde) [40]:

In a 50 mL flask, 4-hydroxybenzaldehyde (6.6 mmol, 0.8 g), potassium carbonate (13 mmol, 1.8 g) and 2-(2-(2- chloroethoxy)ethoxy-ethanol (5.9 mmol, 0.862 mL) were added in 10 mL of dry DMF. The system was kept under stirring, in an atmosphere of N_2 and at 120 °C for 20 h. After this period, the system was cooled to room temperature and the solvent was removed in a rotary evaporator. The obtained residue was suspended in $CHCl_3$, filtered and dried with magnesium sulfate. Purification was carried out on a flash silica chromatographic column using ethyl acetate and methanol (20:1, v/v) as solvent. The product was obtained in the form of a colorless oil with 83 % yield (4.91 mmol, 1.2488 g). ^{1}H NMR (300 MHz, $CDCl_3$) δ 9.88 (s, 1H), 7.83 (d, J = 8.8 Hz, 2H), 7.03 (d, J = 8.7 Hz, 2H), 4.22 ($t_{ap.}$, J = 4.5 Hz, 2H), 3.90 ($t_{ap.}$, J = 6.0 Hz, 2H), 3.79 – 3.68 (m, 6H), 3.62 ($t_{ap.}$, J = 4.5 Hz, 2H). ^{13}C NMR (75 MHz, $CDCl_3$) δ 190.89, 163.74, 131.97, 130.03, 114.86, 72.53, 70.83, 70.27, 69.40, 67.65, 61.65. HRMS m/z for $C_{13}H_{18}O_5$: $[M + Na]^+$ calcd 277.1046; found 277.1051.

b) Synthesis of dipyrromethane (**2**) (2-(2-(2-(4-(di(1H-pyrrol-2-yl) methyl)phenoxy)ethoxy)ethoxy) ethan-1-ol):

The synthesis of the dipyrromethane was adapted by a previously described procedure [41]. In a 50 mL flask, **1** (4.45 mmol, 1.1318 g), pyrrole (86.5 mmol, 6.0 mL) and DCM (15 mL) were added. The system was stirred under an N_2 atmosphere and, subsequently TFA (1.183 mmol, 90.53 μL) was added. The solution immediately turned light brown and was kept under stirring for 2.5 h. The extraction was carried out using 15 mL of $NaHCO_3$ and (15 mL x 3) of dichloromethane. The organic phase was dried with magnesium sulfate and concentrated on the rotary evaporator. The product obtained was purified on a flash silica chromatographic column using a mixture of ethyl acetate and hexane (10:1 v/v) as solvent, obtaining **2** in 73 % yield (3.25 mmol, 1.2013 g) as an oil yellowish. R_f = 0.56 in ethyl acetate and hexane (10:1 v/v). ^{1}H NMR (300 MHz, $CDCl_3$) δ 8.10 (s, 2H), 7.09 (d, J = 8.6 Hz, 2H),

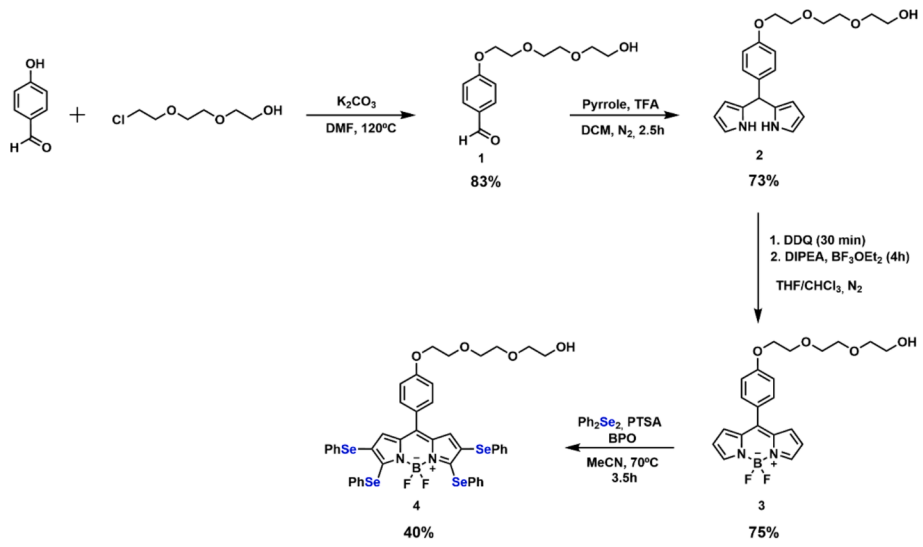

Scheme 1. Synthesis of the seleno-BODIPY.

6.84 (d, $J = 8.7$ Hz, 2H), 6.65 (dd, $J = 4.2$, 2.6 Hz, 2H), 6.13 (dd, $J = 5.8$, 2.8 Hz, 2H), 5.88 – 5.85 (m, 2H), 5.38 (s, 1H), 4.09 ($t_{ap.}$, $J = 4.5$ Hz, 2H), 3.83 ($t_{ap.}$, $J = 4.5$ Hz, 2H), 3.73 – 3.64 (m, 6H), 3.57 ($t_{ap.}$, $J = 4.5$ Hz, 2H), 2.60 (s, 1H). ^{13}C NMR (75 MHz, $CDCl_3$) δ 157.59, 134.68, 132.95, 129.44, 117.17, 114.66, 108.26, 107.01, 72.48, 70.78, 70.35, 69.77, 67.40, 61.72, 43.13. HRMS *m/z* for $C_{21}H_{26}N_2O_4$: $[M + Na]^+$ calcd 393.1785; found 393.1803. IR (ATR, Ge, cm^{-1}): *v* 3386.37412, 2879.06289, 2367.45241, 1612.2179, 1509.03595, 1458.87806, 1246.78184, 1177,99388, 1119.23749, 1066.21343, 1026.08712, 912.87361, 844.08564, 772.43151, 725.13978.

c) Synthesis of BODIPY (**3**) (2-(2-(2-(4-(5,5-difluoro-5H-4 l4,5l4-dipyrrolo[1,2-c:2′,1′-f][1-3]diazaborinin-10-yl)phenoxy)ethoxy) ethoxy)ethan-1-ol):

The synthesis of the BODIPY **3** was adapted by a previously described procedure [42]. In a 500 mL flask, **2** (3 mmol, 1.113 g) was added in 100 mL of $CHCl_3$. The solution was stirred in an N_2 atmosphere. Simultaneously, in another flask, DDQ (3.5 mmol, 0.8 g) was added in 100 mL of $CHCl_3$ and 32 mL of dry THF, under a N_2 atmosphere. The solution containing DDQ was transferred using a cannula to the flask containing dipyrromethane **2**. The reaction mixture was kept under stirring for 30 min. DIPEA (116.5 mmol, 20.35 mL) and $BF_3.OEt_2$ (145.85 mmol, 18 mL) were added successively without any delay time. The reaction medium was kept under stirring at room temperature and in an inert atmosphere for 4 h. Extraction was carried out with saturated potassium bicarbonate solution (200 mL) and chloroform (3 x 200 mL). The organic phase was collected and, after drying with magnesium sulfate, the solvent was removed by rotary evaporation. The reaction crude was purified on a silica flash chromatographic column, using a mixture of ethyl acetate and hexane (4:1 v/v) as eluent, resulting in a red product in 75 % yield (2.25 mmol, 0.935 g). $R_f = 0.30$ (4:1; ethyl acetate and hexane, v/v). ^{1}H NMR (300 MHz, $CDCl_3$) δ 7.92 (s, 2H), 7.53 (d, $J = 8.6$ Hz, 2H), 7.07 (d, $J = 8.7$ Hz, 2H), 6.96 (d, $J = 4.1$ Hz, 2H), 6.55 (broad dd, $J = 4.0$, 1.5 Hz, 2H), 4.24 ($t_{ap.}$, $J = 4.5$ Hz, 2H), 3.93 ($t_{ap.}$, $J = 4.5$ Hz, 2H), 3.79 – 3.71 (m, 6H), 3.64 ($t_{ap.}$, $J = 4.5$ Hz, 2H), 2.64 (s, 1H). ^{13}C NMR (75 MHz, $CDCl_3$) δ 161.23, 147.35, 143.44, 134.81, 132.42, 131.40, 126.52, 118.35, 114.65, 72.54, 70.87, 70.33, 69.55, 67.62, 61.75. The melting point was not possible to be obtained since the product is a wax-like material. HRMS *m/z* for $C_{21}H_{23}BF_2N_2O_4$: $[M + Na]^+$ calcd 439.1615; found 439.1612. IR (ATR, Ge, cm^{-1}): v 2932.08695, 1602.18632, 1543.42993, 1413.01942, 1388.65701, 1256.81342, 1182.29312, 1116.37132, 1074.81193, 980.22848, 912.8736, 776.73075, 743.76986.

d) Synthesis of BODIPY (**4**) 2-(2-(2-(4-(5,5-difluoro-2,3,7,8-tetrakis (phenylselanyl)-5H-4 l4,5l4-dipyrrolo[1,2-c:2′,1′-f][1-3]diazaborinin-10-yl)phenoxy)ethoxy)ethoxy)ethan-1-ol:

BODIPY **3** (0.85 mmol, 354 mg), diphenyl diselenide (2.13 mmol, 664 mg), BPO (2.13 mmol, 516 mg) and ACN (32 mL) were added to a round-bottom flask (50 mL). A solution of *p*-TSA (1.38 mmol, 237.64 mg) in MeCN (10 mL) was added to the reaction flask, and the solution was stirred under heating (70 °C) for 3.5 h. The reaction was quenched by adding 50 mL of distilled water and then, extracted with DCM (3 x 50 mL). The organic phase obtained was dried over anhydrous $MgSO_4$, filtered, and concentrated at a rotary evaporator. The purification was performed by a C18-reversed phase silica column chromatography using 9:1 MeCN/H_2O (v/v) to afford BODIPY **4** (349.9 mg, 40 %) as a dark green solid. $R_f = 0.16$ (9:1; MeCN/H_2O, v/v). ^{1}H NMR (300 MHz, $CDCl_3$) δ 7.65 – 7.57 (m, 4H), 7.32 (d, $J = 8.7$ Hz, 2H), 7.28 – 7.10 (m, 17H) [obs: together with residual $CHCl_3$], 6.91 (d, $J = 8.7$ Hz, 2H), 6.76 (s, 2H), 4.15 ($t_{ap.}$, $J = 4.5$ Hz, 2H), 3.87 ($t_{ap.}$, $J = 4.5$ Hz, 2H), 3.76 – 3.67 (m, 6H), 3.61 ($t_{ap.}$, $J = 3$ Hz, 2H). ^{13}C NMR (75 MHz, $CDCl_3$) δ 161.04, 151.14, 140.08, 136.74, 134.91, 133.90, 132.26, 131.65, 131.16, 129.82, 129.26, 129.15, 128.03, 127.25, 127.09, 125.61, 114.60, 72.45, 70.82, 70.29, 69.47, 67.51, 61.72. ^{77}Se NMR (57 MHz, $CDCl_3$, using Ph_2Se_2 as external standard) δ 378.10, 311.65. The melting point was not possible to be obtained since the product is a wax-like material. HRMS (*m/z*): $[M + Na]^+$ for $C_{45}H_{39}BF_2N_2O_4Se_4$ = 1060.9531 (−2.7 ppm). Calculated $[M + Na]^+$ for $C_{45}H_{39}BF_2N_2O_4Se_4$ = 1060.955933. $[M]^+$ for $C_{45}H_{39}BFN_2O_4Se_4$ = 1018.9647 (−3.0 ppm). Calculated $[M]^+$ for $C_{45}H_{39}BFN_2O_4Se_4$ = 1018.967766. IR (ATR, Ge, cm^{-1}): v 2874.76364, 1603.6194, 1572.09158, 1531.96527, 1474.64197, 1306.97131, 1225.38033, 1220.98635, 1177.99388, 1092.00892, 1020.35479, 997.42547, 904.2751, 841.21947, 733.73828, 689.31272.

3. Results and discussion

3.1. Design, synthesis and structure characterization of the BODIPY 4

In this work, we designed and synthesized a new BODIPY derivative (**4**) containing four phenylselenide groups through a new synthetic methodology developed in our group for acting as a fluorescent probe for CN^-, F^-, and OH^-. In the first step, the 4-hydroxibenzaldehyde was submitted to reaction with 2-(2-(2-chloroethoxy)ethoxy-ethanol, allowing the formation of the aldehyde **1** containing 3 polyethylene glycol (PEG) units, aiming to increase the solubility of the final BODIPY in more polar solvents and facility the purification process. The synthesis of BODIPY core was carried out based on an adaptation of a previously

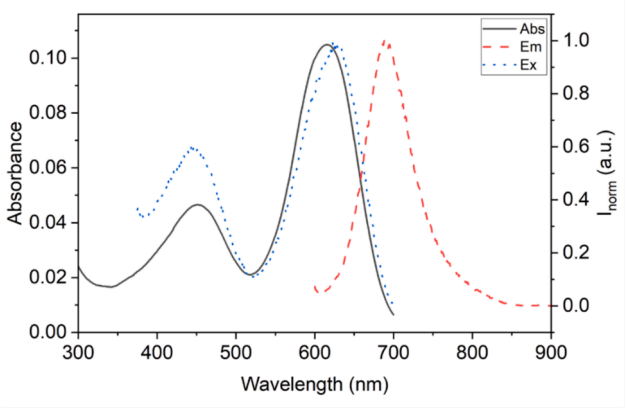

Fig. 1. Absorption, normalized emission and normalized excitation spectra of compound **4** in THF. (T = 298 K; [BODIPY **4**] = 2 μmol/L; λ_{em} = 720 nm; λ_{exc} = 590 nm; slit = 5.0 nm).

Table 1
Photophysical data of compound **4** in THF at 298 K.

Absorption data			Emission data			
λ_{abs} (nm)	ε (L.mol^{-1}.cm^{-1})	$Fwhm_{abs}$ (nm)	λ_{em} (nm)	Stokes shift (nm)	$Fwhm_{em}$ (nm)	Φ
451 615	22861.03 53398.52	125.76 94.53	688	73	67.77	<0.01

reported procedures [41,42] and consists of the reaction of compound **1** with pyrrole, using TFA as a catalyst, leading to the formation of dipyrromethane (**2**) in 73 % yield. Next, a sequence of an oxidation reaction with DDQ followed by complexation with BF_3.OEt in the presence of DIPEA, was performed, leading to the formation of product **3** in 75 % yield. The post functionalization of BODIPY **3** was conducted in one step, using Ph_2Se_2, BPO, and *p*-TSA in MeCN resulting in the desired compound **4** in 40 % yield (Scheme 1). The structures of all products were confirmed by NMR ^{1}H, ^{13}C, and ^{77}Se (for BODIPY **4**), HRMS and infrared spectroscopy (Figs. S31-S54). Compound **4** was also characterized by UV–visible absorption and fluorescence emission spectroscopy (Fig. 1).

The optimization of the selenylation reaction was previously performed using another BODIPY core (**5**) as a model (Table S2). The reactant concentrations, temperature, and solvent were varied having entry 7 as the optimal condition. It was verified that using compound **3** under these conditions (T = 50 °C and 1.25 equiv. of Ph_2Se_2 in relation to **3**), the BODIPY core becomes more activated due to the presence of the PEG-derived substituent, making it possible to obtain, after 1 h of reaction, BODIPYs derivatives containing 2, 3 and 4 selenium groups (BODIPYs **8** (20 %), **9** (6 %), and **4** (22 %), respectively), not being observed the formation of BODIPY with one "SePh" group (Scheme S1). Based on these results, an optimal condition was established for the selenilation step using BODIPY **3** as substrate, by increasing the temperature to 70 °C and the amount of Ph_2Se_2 to 2.5 equiv. giving rise to the product of interest **4** in 40 % yield (Scheme 1).

This new methodology, using an electrophilic reagent of selenium generated *in situ*, is advantageous since it does not require prior functionalization of the BODIPY nucleus with halogens or other leaving groups, as is commonly reported in the literature [32,34,35]. This allows a direct functionalization with "PhSe" group, in a simple and practical procedure, and the insertion of two, three or four selenium groups, being a very versatile method. Also, the proportion between products can be controlled by varying reaction time, temperature, and proportion of the selenium reagent.

The seleno-functionalization strategy of the BODIPY nucleus was carried out since selenium leads to the suppression of the compound's fluorescence, due to the heavy atom effect [43]. In this way, this allows the chalcogenated group to be used as a recognition site for certain analytes, allowing it to be applied as an on/off fluorescent sensor. When in the presence of an analyte that interacts with the selenium-containing groups specifically, BODIPY fluorescence can be restored in a turn-on fluorescence process. Furthermore, chalcogenated BODIPYs exhibit low background fluorescence, which is a desirable characteristic in the design of a new sensor. Continuing our group's interest in the synthesis and application of new sensors for detecting analytes of environmental and biological interest [44,45], in the present work we designed BODIPY **4** and decided to study its interaction with anions of environmental interest.

3.2. Photophysical characterization of BODIPY 4

The photophysical properties of BODIPY **4** were investigated in THF. The compound presented optimal solubility in this solvent, and it was

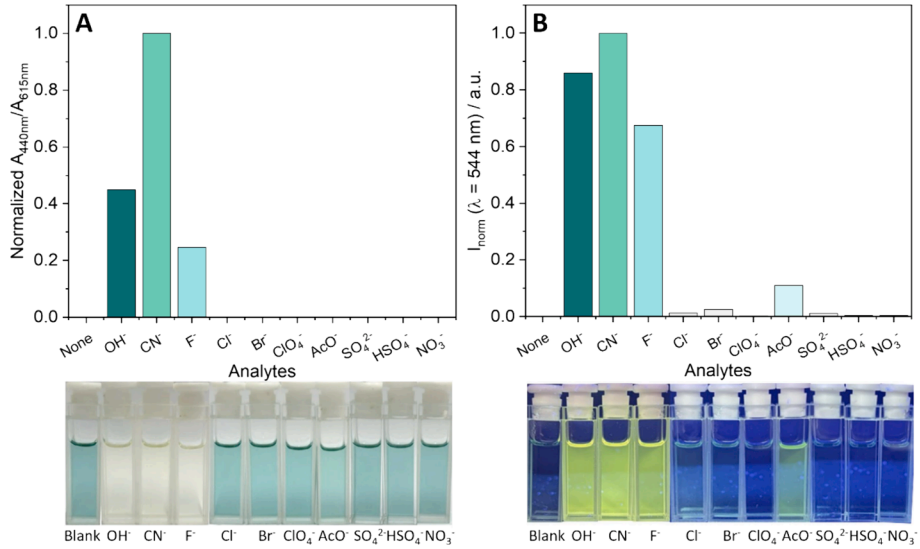

Fig. 2. A) Normalized absorbance A_{440nm}/A_{615nm} and **B)** Normalized intensity (λ = 541 nm) of **4** (7.0 μM) in THF, upon addition of analytes (20 equiv.,140 μM), after 10 min of reaction, λ_{ex} 440 nm, slit 1.5 nm. Images of solutions of BODIPY **4** after addition of analytes under visible light and under UV light.

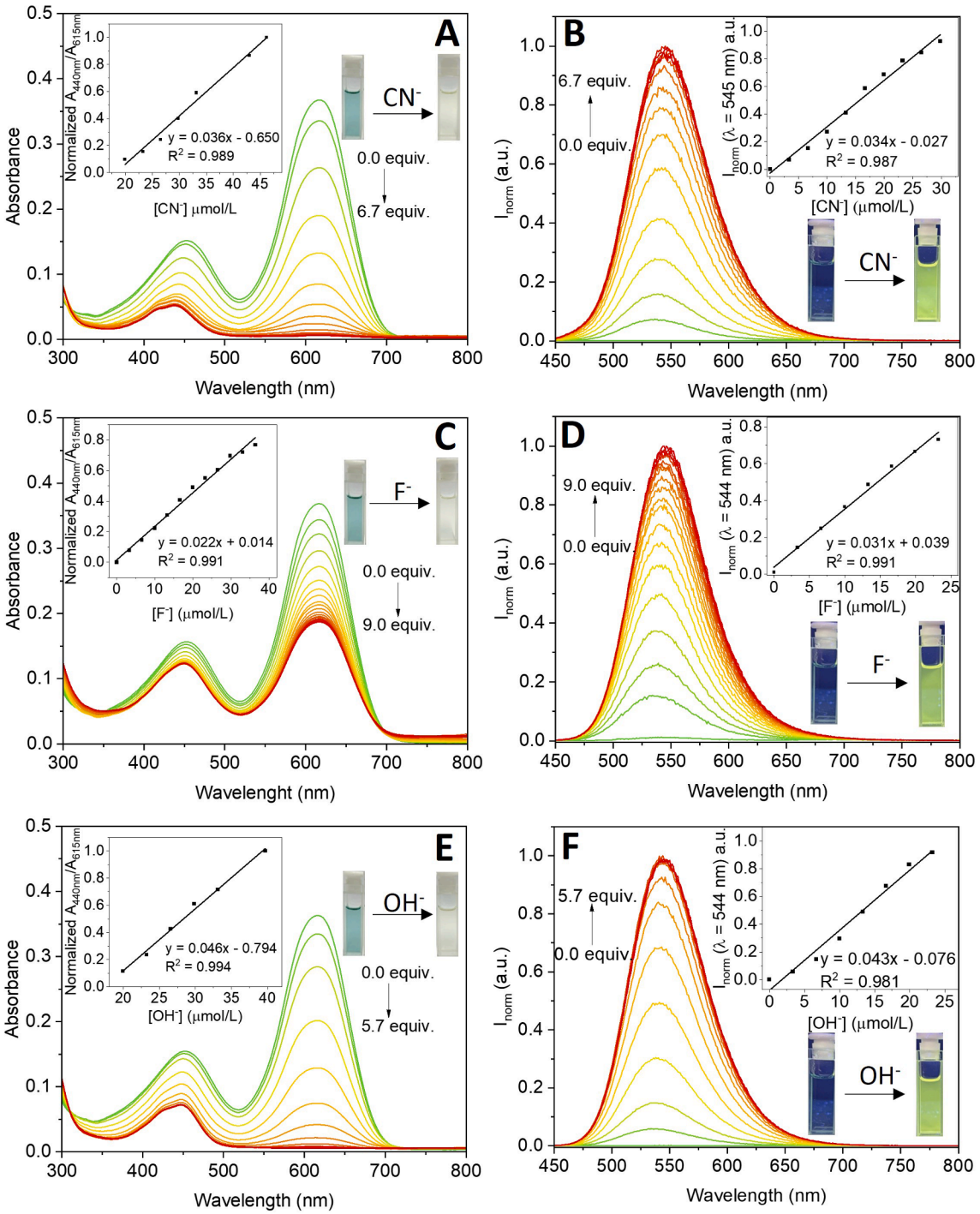

Fig. 3. Spectrophotometric titrations of **4** in THF with increasing amounts of **A)** CN^-, **C)** F^- and **E)** OH^-. Inset: Normalized A_{440nm}/A_{615nm} as a function of **A)** [CN^-] (y = 0.036x–0.650, $R^2 = 0.989$), **C)** [F^-] (y = 0.022x + 0.014, $R^2 = 0.991$) or **E)** [OH^-] (y = 0.046x–0.794, $R^2 = 0.994$). Spectrofluorimetric titrations of **4** in THF with increasing amounts of **B)** CN^-, **D)** F^- and **F)** OH^-. Inset: Emission at 545 nm as function of **B)** [CN^-] (y = 0.034x–0.027, $R^2 = 0.987$) and emission at 544 nm as function of **D)** [F^-] (y = 0.031x + 0.039, $R^2 = 0.991$) or **F)** [OH^-] (y = 0.043x – 0.076, $R^2 = 0.981$) and images of visual color change under visible light and under UV light upon addition of each analyte. Condition: T = 298 K, [BODIPY] = 7.0 µmol/L, λ_{ex} = 440 nm, slit = 1.5 nm.

obtained absorption, emission, and excitation spectra (Fig. 1). From the absorption spectrum, it was possible to observe the presence of 2 transition bands at 615 nm (ε = 53398.52 $L.mol^{-1}.cm^{-1}$) and 451 nm (ε = 22861.03 $L.mol^{-1}.cm^{-1}$) (Table 1), which is a spectral profile characteristic of BODIPYs [46–49]. The highest band (λ = 615 nm) corresponds to the vibrational transitions 0–0 and 0–1 of the strong $S_0 \rightarrow S_1$ transition. In some cases, the 0–1 vibrational band appears as a shoulder at the $S_0 \rightarrow S_1$ transition, which can be more or less pronounced depending on the molecule [46,47]. In the case of BODIPY **4**, due to the presence of four heavy atoms (4 groups containing selenium), the band is wider ($Fwhm_{abs}$ = 94.53 nm) and the presence of shoulder is not observed [35]. The weaker band of absorption (λ = 451 nm) can be attributed to the transition $S_0 \rightarrow S_n$ ($n \geq 2$) [46,47]. The emission spectrum was obtained as a mirror image of the absorption spectrum, with the emission maximum at 688 nm, corresponding to the $S_1 \rightarrow S_0$ transition. The BODIPY **4** presented a weak fluorescence intensity with a low

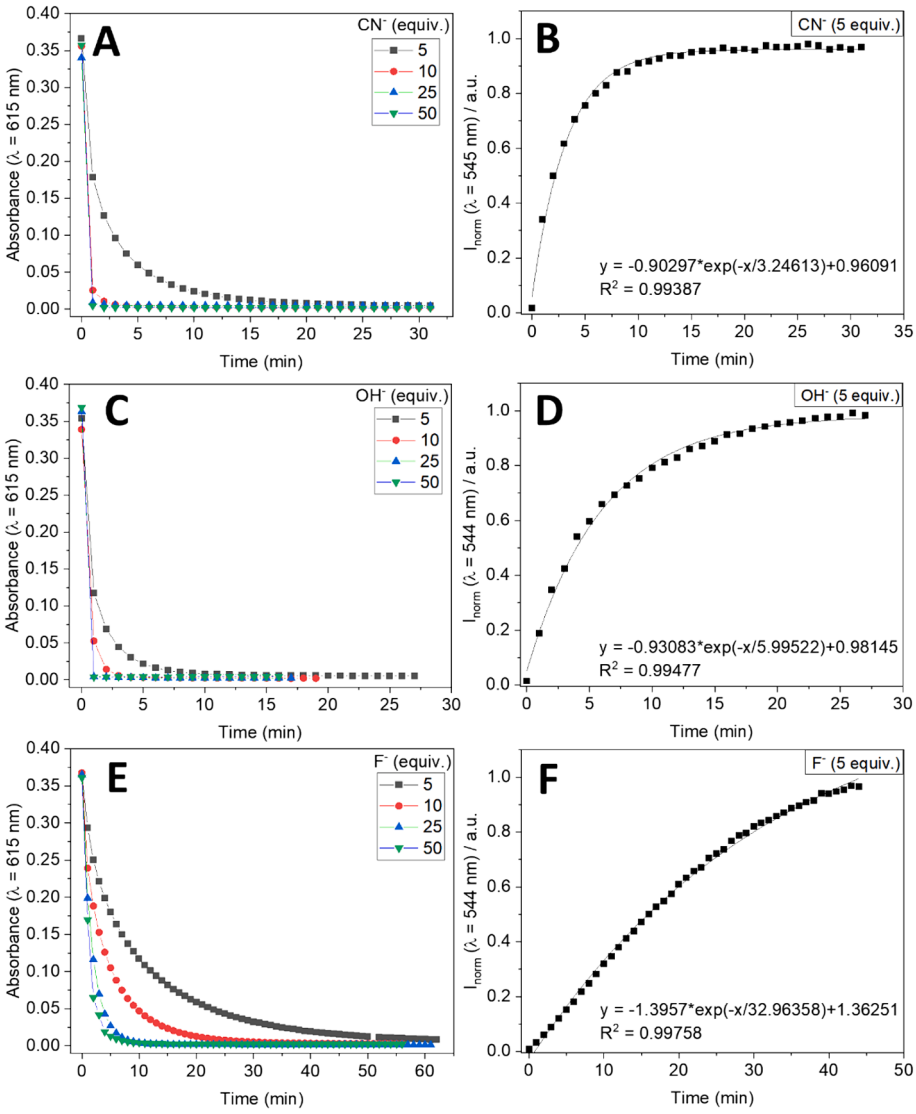

Fig. 4. Time-dependent response of the absorbance at λ = 615 nm of BODIPY **4** after addition of different concentrations (5, 10, 25 and 50 equiv.) of **A)** CN^-, **C)** OH^- and **E)** F^-. Time-dependent response of the emission at λ = 545 nm or λ = 544 nm of BODIPY **4** after addition of 5 equiv. of **B)** CN^-, **D)** OH^- and **F)** F^-. Conditions: T = 298 K; [BODIPY **4**] = 7 μmol/L in THF. λ_{ex} = 440 nm, slit 1.5 nm.

fluorescence quantum yield (Φ < 0.01). The absence of fluorescence leads us to the hypothesis that the *Photoinduced electron Transfer (PeT)* [38,50,51] process caused by the electron-donating effect of the phenylselenide groups to the chromophoric nucleus of BODIPY is involved, as previously report for other seleno-BODIPYs derivatives [29,52–54].

3.3. Anion sensing studies with BODIPY *4*

A screening with 10 selected anions (OH^-, CN^-, F^-, Cl^-, Br^-, ClO_4^-, AcO^-, SO_4^{2-}, HSO_4^-, NO_3^-) from tetrabutylammonium salts was conducted in THF through absorption spectra (Fig. S1). It was possible to see a differential response of **4** for CN^-, F^- and OH^-, accompanied by a color change from blue to yellow fluorescence (Fig. 2). From a spectral point of view, a decrease in absorbance at λ = 615 nm is observed and the final spectra obtained presents a maximum wavelength (λ_{max}) at 440 nm for CN^-, F^- and OH^-(Fig. S1). Ratiometric analysis considering the ratio A_{440nm}/A_{615nm} was also conducted, making it possible to better observe the selectivity for these analytes (Fig. 2A). The reactions were also accompanied by fluorescence spectra (Fig. S2). Compound **4** is non-fluorescent in THF, as expected, due to chalcogenated groups in the structure. When **4** is in the presence of excess amounts of OH^-, CN^-, or F^-, occurs an instantaneous appearance of fluorescence in a turn-on fluorescence process, with an λ_{max} = 544 nm, presenting a predominant response for these analytes (Fig. 2, B). It was also observed a minimal response for AcO^- under these conditions, by fluorescence.

The spectrofluorimetric and spectrophotometric (Fig. 3) titrations of sensor **4** with CN^-, OH^- and F^- were conducted. It was possible to notice the appearance of fluorescence emission intensity when in the presence of CN^-, F^-, or OH^-, with maximum emission at 545 nm (for CN^-) and 544 nm (for F^- and OH^-), in a turn-on fluorescence process. A hypsochromic shift of 143/144 nm was observed on emission spectra, compared to the residual fluorescence of compound **4** (λ = 688 nm), as expected due to the possible inhibition of the PeT process. From the titrations, it was possible to obtain a linear correlation between the fluorescence intensity and the concentration of CN^-, F^- and OH^- (Fig S3-S5). Limits of detection (LOD) and quantification (LOQ) were obtained for CN^- (LOD = 26.26 nmol/L; LOQ = 87.53 nmol/L), F^- (LOD = 43.05 nmol/L; LOQ = 143.49 nmol/L), and OH^- (LOD = 8.64 nmol/L; LOQ = 28.79 nmol/L), showing that the probe **4** is an excellent sensor for these analytes. The fluorescence quantum yields of the final products were also obtained, using benzothioxanthene imide (BTI) in chloroform as standard [55], resulting in 57 % for the product with OH^-, 50 % for CN^-,

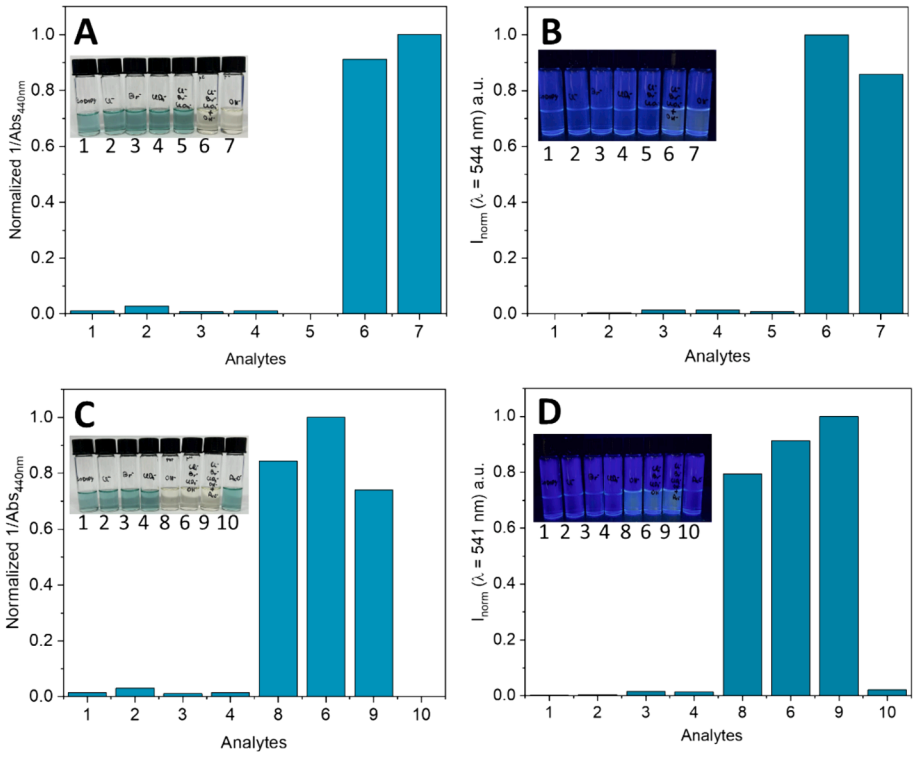

Fig. 5. **A)** Normalized absorption and **b)** normalized emission of BODIPY **4** in the presence of each analyte (20 equiv. for Cl^-, Br^-, ClO_4^- after 20 min of adding OH^- (5 equiv.) **c)** Normalized absorption and **d)** normalized emission of **4** in the presence of each analyte (20 equiv. for Cl^-, Br^-, ClO_4^-, OH^- after 20 min of adding AcO^- (5 equiv.). Analytes: **1** = Blank; **2** = Cl^- (20 equiv.); **3** = Br^- (20 equiv.); **4** = ClO_4^- (20 equiv.); **5** = Cl^- + Br^- + ClO_4^- (20 equiv.); **6** = Cl^- + Br^- + ClO_4^- (20 equiv.) + OH^- (5 equiv.); **7** = OH^- (5 equiv.); **8** = OH^- (20 equiv.); **9** = Cl^- + Br^- + ClO_4^- + OH^- (20 equiv.) + AcO^- (5 equiv.); **10** = AcO^- (5 equiv.). Conditions: T = 298 K, [BODIPY] = 7.0 μmol/L, THF, λ_{ex} = 440 nm, slit 1.5 nm.

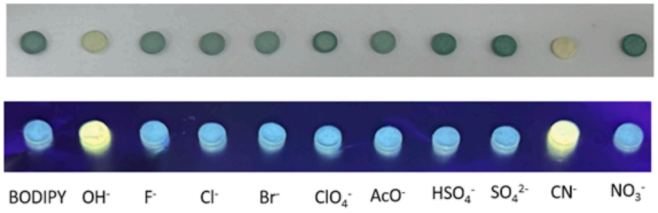

Fig. 6. Images of paper discs after immersion in solutions containing BODIPY **4** and each anion, after 1 min reaction, under visible and UV light. [BODIPY **4**] = 1.0×10^{-4} mol/L and [anions] = 5.0×10^{-3} mol/L (50 equiv.) in THF.

and 11 % for F^-.

The LOD obtained for cyanide was much lower than some previously reported (Table S1) and 73 times lower compared with the maximum level permitted by WHO for CN^- levels (1.9 μM) in drinking water [8]. Based on this information and the results obtained, we can confirm that our sensor is highly sensitive for CN^- detection. In the case of F^- the LOD obtained was close to some reported results for other probes and, in some cases, lower than others reported (Table S1). Fluorescent probes for hydroxide are not commonly reported, and most sensors are for hydroxyl radicals [56].

Spectrophotometric titrations were also conducted (Fig. 3), obtaining a linear correlation between the ratio A_{440nm}/A_{615nm}, allowing sensor **4** to be used for ratiometric detection and quantification of these analytes (Figs. S6-S8). Monitoring the absorption at two different wavelengths allows improvement in the accuracy and sensitivity of the

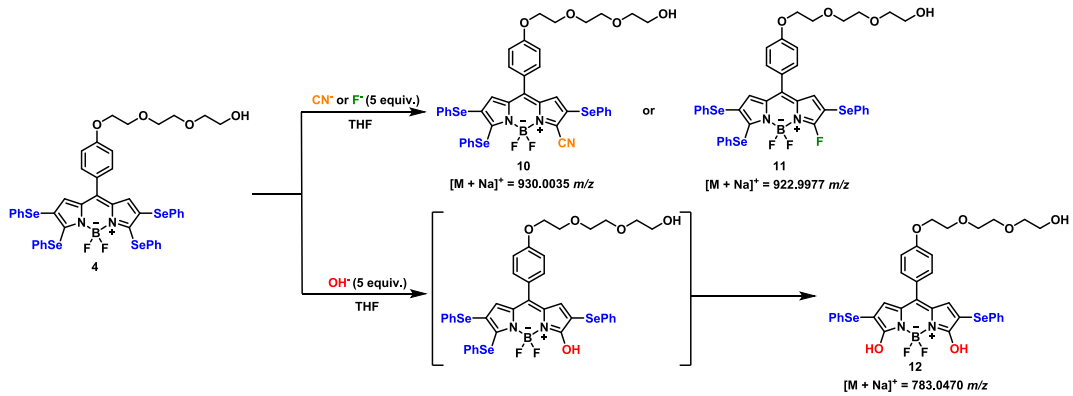

Scheme 2. Proposed reaction of BODIPY **4** with CN^-, F^-, and OH^-.

experiment. It was observed a decrease at the larger band of BODIPY **4** (λ = 615 nm), and the final products presented a band at λ = 440 nm, accompanied by the color change of the solution from blue to yellow (Fig. 3). The decrease in absorption at λ = 615 nm was proportional to the increase in fluorescence emission of the **4** when in the presence of CN^-, F^- or OH^- (Figs. S9-S11).

Time-dependent response of BODIPY **4** in the presence of different concentrations (5, 10, 25, and 50 equiv.) of analytes CN^-, OH^- and F^- were obtained by absorption (Fig. S12-S14) and emission spectra (Figs. S15-S17). The results were monitored through the consumption of reagent by absorption (λ = 615 nm) and formation of the product by emission (λ = 545 nm for CN^- and λ = 544 nm for OH^- and F^-). It was observed that the reactions of **4** with CN^- (5 equiv.) and OH^- are faster (taking around 10–15 min for stabilization) than the reaction with F^- (45–50 min) in the same concentration (Fig. 4). Time-dependent response of BODIPY **4** in the presence of the other analytes studied were monitored for 30 min and no significant variation was observed (Figs. S18-S21). Comparative analysis of response time of **4** with CN^-, OH^-, F^-, and AcO^-, showed that the reaction with acetate is much slower than the others (Fig. S22).

In order to study the selectivity of BODIPY **4** for the detection of CN^-, F^- and OH^-, an interference study was carried out. Initially, a scan was performed to verify the occurrence of a reaction between BODIPY **4** with OH^- when in the presence of each analyte that did not react with BODIPY **4** in the previous screening in Fig. 2. In this way, 5 equiv. of OH^- were added to solutions containing 20 equiv. of the anions Cl^-, Br^-, ClO_4^-, AcO^-, SO_4^{2-}, HSO_4^- and NO_3^- with BODIPY **4** (7 μmol/L), separately. The occurrence of reaction with OH^-, even when in the presence of Cl^-, Br^-, ClO_4^-, was immediately observed, accompanied by a color change from blue to light yellow (Fig. S25). After 1 h of reaction, no significant change was observed for the solutions containing AcO^-, SO_4^{2-}, HSO_4^- and NO_3^-. After 3 h of reaction, a different response was noted in the solution containing OH^- and AcO^-, appearing an intense yellow color, suggesting that a different product was formed when in the presence of AcO^- (Fig S25). After 24 h reaction, absorption (Fig. S26) and emission spectra (Fig. S27) of these solutions were performed and, visually, higher fluorescence intensity values were obtained when BODIPY **4** was in the presence of AcO^-, SO_4^{2-} or HSO_4^-, indicating that different products were obtained compared to the one obtained with OH^-. Therefore, a small variation was observed when analyses were conducted in the presence of Cl^-, Br^- or ClO_4^-, without noticeable interference.

It was also found that BODIPY **4** reacts with OH^- (5 equiv.) even in the presence of mixed Cl^-, Br^-, and ClO_4^- (20 equiv. of each analyte) (Fig. 5). The results were measured by absorption and emission spectra (Fig. S30). It is possible to verify that the reaction occurs normally under these conditions, with a small increase in the emission intensity when Cl^-, Br^- and ClO_4^- are mixed in the solution (Fig. 5A, B). Control experiments with the addition of anions separately were also carried out. Knowing that acetate was a potential interference in the reaction of **4** with OH^-, a similar experiment was carried out adding 5 equiv. of AcO^- to a solution containing 20 equiv. of Cl^-, Br^-, ClO_4^-, OH^-. (Fig. 5C, D). Higher emission intensity value was obtained comparing to the control experiments containing only OH^- (20 equiv.) or Cl^-, Br^-, ClO_4^-, OH^- mixed. This probably occurs due to the product obtained in the reaction between BODIPY **4** and AcO^- having a higher fluorescence intensity than the product with OH^- and slower kinetics. After 48 h of reaction, the presence of intense yellow fluorescence was clearly observed in the control solution containing only AcO^- (20 equiv.) (Fig. S28).

Paper discs were impregnated with final solutions containing BODIPY **4** (1.0×10^{-4} mol/L) and 50 equiv. of each analyte, making it possible to visualize a different response for OH^- and CN^- both under visible and UV light in solid state, immediately after reaction. It was not possible to visually observe any changes for F^- due to slower kinetics (Fig. 6).

3.4. Study by mass spectrometry and proposed sensing mechanism

To investigate the reaction of BODIPY **4** with the anions CN^-, F^-, and OH^-, high-resolution mass spectrometry (ESI-micrOTOF-MS) (**Figs. S66-S76**) were carried out. It was possible to conclude that an unexpected Aromatic Nucleophilic Substitution reaction occurs, in which the anions act as nucleophiles leading to the substitution of seleno-phenyl groups (Scheme 2). It was observed that in the reaction with CN^- or F^- (5 equiv.), there is a monosubstitution of a SePh group at positions 3 or 5 of the nucleus (resulting in compounds **10** or **11**, respectively, whereas when in the presence of OH^-, a double substitution is observed (resulting in compound **12**). This was confirmed by the identification of mass peaks relative to [BODIPY **10** + Na]$^+$ = 930.0035 *m/z* (m/z_{calcd} = 930.002773), [BODIPY **11** + Na]$^+$ = 922.9977 *m/z* (m/z_{calcd} = 922.998059), and [BODIPY **12** + Na]$^+$ = 783.0470 *m/z* (m/z_{calcd} = 783.047848). It was also verified that the isotope pattern for all these cluster are very similar to the respective theoretical analysis. A similar Aromatic Nucleophilic Substitution reaction has already been reported for a seleno-coumarin, using biothiols as nucleophiles and having the seleno-phenyl as the leaving group [43]. Furthermore, it is known that positions 3 and 5 of the BODIPY nucleus are more susceptible to substitution reactions compared to positions 2 and 6, being the halogenation of positions 3 and 5 before a nucleophilic substitution reaction a commonly reported strategy [51].

4. Conclusions

A novel tetraseleno-BODIPY was designed and synthesized in a direct functionalization of BODIPY core using a new methodology of synthesis. The new procedure uses diphenyl diselenide, benzoyl peroxide, and *p*-TSA in ACN resulting in compounds with two to four selenium groups. The new chemical sensor was used for colorimetric and fluorimetric detection of CN^-, F^-, and OH^- anions at ultra-low detection limits, presenting high sensitivity, ratiometric response in a turn-on fluorescence process. Low detection limits (26.26 nM for CN^-, 43.05 nM for F^-, and 8.64 nM for OH^-) were obtained for these analytes. Competition studies demonstrated that BODIPY **4** can detect OH^- in the presence of Cl^-, Br^- and ClO_4^- without interference. It was possible to concluded that BODIPY **4** reacts with CN^-, OH^-, and F^- through Aromatic Nucleophilic Substitution reaction, resulting in monosubstituted products (for CN^- and F^-) and disubstituted product for OH^-.

CRediT authorship contribution statement

Beatriz S. Cugnasca: Conceptualization, Formal analysis, Investigation, Methodology, Software, Validation, Writing – original draft, Writing – review & editing. **Frederico Duarte:** Investigation, Validation, Writing – review & editing. **João L. Petrarca de Albuquerque:** Investigation, Validation, Visualization, Writing – review & editing. **Hugo M. Santos:** Formal analysis, Investigation, Methodology, Software, Validation, Writing – original draft, Writing – review & editing. **José Luis Capelo-Martínez:** Funding acquisition, Visualization, Writing – review & editing. **Carlos Lodeiro:** Conceptualization, Funding acquisition, Methodology, Project administration, Supervision, Validation, Writing – original draft, Writing – review & editing. **Alcindo A. Dos Santos:** Conceptualization, Funding acquisition, Methodology, Project administration, Supervision, Validation, Writing – original draft, Writing – review & editing.

Declaration of competing interest

The authors declare the following financial interests/personal relationships which may be considered as potential competing interests: Carlos Lodeiro reports financial support was provided by Proteomass Scientific Society. If there are other authors, they declare that they have no known competing financial interests or personal relationships that

could have appeared to influence the work reported in this paper.

Acknowledgements

Beatriz S. Cugnasca thanks FAPESP (2019/07634-1 and 2023/01092-8), Brazil, for Ph.D. scholarship and CNPq (141855/2019-3), Brazil. Alcindo A. Dos Santos thanks FAPESP (2018/24434-3) and CNPq. João L. Petrarca de Albuquerque thanks FAPESP (2020/04782-7). All authors thank FAPESP, CNPq, and CAPES for financial support and the Institute of Chemistry of University of São Paulo, Brazil for research structure and support. F.D. thanks to FCT/MCTES (Portugal) for his doctoral grant 2021.05161.BD. HMS acknowledges the Associate Laboratory for Green Chemistry-LAQV (LA/P/0008/2020) funded by FCT/MCTES for his research contract. This work received support and help from FCT/MCTES (LA/P/0008/2020 DOI 10.54499/LA/P/0008/2020, UIDP/50006/2020 DOI 10.54499/UIDP/50006/2020 and UIDB/50006/2020 DOI 10.54499/UIDB/50006/2020), through national funds. PROTEOMASS Scientific Society (Portugal) is acknowledged by the funding provided through the General Funding Grant 2023-2024, and by the funding provided to the Laboratory for Biological Mass Spectrometry Isabel Moura (#PM001/2019 and #PM003/2016).

Appendix A. Supplementary data

Supplementary data to this article can be found online at https://doi.org/10.1016/j.jphotochem.2024.115881.

References

[1] A.B. Aletti, D.M. Gillen, T. Gunnlaugsson, Luminescent/colorimetric probes and (chemo-) sensors for detecting anions based on transition and lanthanide ion receptor/binding complexes, Coord. Chem. Rev. 354 (2018) 98–120, https://doi.org/10.1016/j.ccr.2017.06.020.
[2] A. Pal, M. Karmakar, S.R. Bhatta, A. Thakur, A detailed insight into anion sensing based on intramolecular charge transfer (ICT) mechanism: A comprehensive review of the years 2016 to 2021, Coord. Chem. Rev. 448 (2021), https://doi.org/10.1016/j.ccr.2021.214167.
[3] P.A. Gale, C. Caltagirone, Fluorescent and colorimetric sensors for anionic species, Coord. Chem. Rev. 354 (2018) 2–27, https://doi.org/10.1016/j.ccr.2017.05.003.
[4] N. Kuyucak, A. Akcil, Cyanide and removal options from effluents in gold mining and metallurgical processes, Miner. Eng. 50–51 (2013) 13–29, https://doi.org/10.1016/j.mineng.2013.05.027.
[5] D. Schrenk, et al., Evaluation of the health risks related to the presence of cyanogenic glycosides in foods other than raw apricot kernels, EFSA J. 17 (2019).
[6] K. Abraham, T. Buhrke, A. Lampen, Bioavailability of cyanide after consumption of a single meal of foods containing high levels of cyanogenic glycosides: a crossover study in humans, Arch Toxicol 90 (2016) 559–574.
[7] F. Wang, L. Wang, X. Chen, J. Yoon, Recent progress in the development of fluorometric and colorimetric chemosensors for detection of cyanide ions, Chem. Soc. Rev. 43 (2014) 4312–4324, https://doi.org/10.1039/c4cs00008k.
[8] Guidelines for Drinking-Water Quality, World Health Organization, Geneva, 1996.
[9] M. Kleerekoper, The role of fluoride in the prevention of osteoporosis, Endocrinol. Metab. Clin. North Am. 27 (2) (1998) 441–452, https://doi.org/10.1016/s0889-8529(05)70015-3.
[10] X. Wu, et al., Highly sensitive ratiometric fluorescent paper sensors for the detection of fluoride ions, ACS Omega 4 (2019) 4918–4926.
[11] P. Denbesten, W. Li. *Chronic Fluoride Toxicity: Dental Fluorosis. Monogr Oral Sci. Basel, Karger* vol. 22 (2011).
[12] A. Attar, et al., Amperometric inhibition biosensors based on horseradish peroxidase and gold sononanoparticles immobilized onto different electrodes for cyanide measurements, Bioelectrochemistry 101 (2015) 84–91.
[13] H.I. Kang, H.S. Shin, Derivatization method of free cyanide including cyanogen chloride for the sensitive analysis of cyanide in chlorinated drinking water by liquid chromatography-tandem mass spectrometry, Anal. Chem. 87 (2015) 975–981.
[14] W. Wu, et al., Rapid measurement of free cyanide in liquor by ion chromatography with pulsed amperometric detection, Food Chem. 172 (2015) 681–684.
[15] Toxicological Profile for Fluorides, Hydrogen Fluoride, and Fluorine. Atlanta (GA): Agency for Toxic Substances and Disease Registry (US); 2003 Sep. PMID: 38079503.
[16] X. Li, X. Liu, A sensitive probe of meso-cyanophenyl substituted BODIPY derivative as fluorescent chemosensor for the detection of multiple heavy metal ions, J. Fluoresc. (2024), https://doi.org/10.1007/s10895-024-03581-4.
[17] X. Wang, et al., Fluorescent probes for disease diagnosis, Chem. Rev. (2024), https://doi.org/10.1021/acs.chemrev.3c00776.
[18] X. Li, X. Liu, F. Li, Configuration of super-fast Cu^{2+}-responsive chemosensor by attaching diaminomaleonitrile to BODIPY scaffold for high-contrast fluorescence imaging of living cells, Spectrochim. Acta A Mol. Biomol. Spectrosc. 304 (2024).
[19] Z. Xu, X. Chen, H.N. Kim, J. Yoon, Sensors for the optical detection of cyanide ion, Chem. Soc. Rev. 39 (2010) 127–137.
[20] Y. Hao, et al., A highly selective and ratiometric fluorescent probe for cyanide by rationally altering the susceptible H-atom, Talanta 176 (2018) 234–241.
[21] W. Saiyasombat, U. Eiamprasert, T. Chantarojsiri, K. Chainok, S. Kiatisevi, Bis-BODIPY-based fluoride and cyanide sensor mediated by unconventional deprotonation of C–H proton, Dyes Pigm. 206 (2022).
[22] R. Ali, S.K. Dwivedi, H. Mishra, A. Misra, Imidazole-coumarin containing D – A type fluorescent probe: Synthesis photophysical properties and sensing behavior for F− and CN− anion, Dyes Pigm. 175 (2020).
[23] H. Xu, O.A. Sadik, Design of a simple optical sensor for the detection of concentrated hydroxide ions in an unusual pH range, Analyst 125 (2000) 1783–1786.
[24] N. Thakur, S.A. Kumar, A.K. Pandey, S.D. Kumar, A.V.R. Reddy, Optode sensor for on-site detection and quantification of hydroxide ions in highly concentrated alkali solutions, RSC Adv. 5 (2015) 72893–72899.
[25] L.R. Allaan, Z. Xue, Optical sensors for the determination of concentrated hydroxide, Anal. Chem. 72 (2000) 1078–1083.
[26] A. Safavi, H. Abdollahi, Optical sensor for high PH values, Anal. Chim. Acta 367 (1–3) (1998) 167–173, https://doi.org/10.1016/S0003-2670(98)00079-8.
[27] T. Imato, N. Ishibashi, Flow injection analysis of concentrated aqueous solution strong acids and bases, Anal. Sci. 1 (1985) 481–482, https://doi.org/10.2116/analsci.1.481.
[28] S.Y. Li, et al., A novel diarylethene-hydrazinopyridine-based probe for fluorescent detection of aluminum ion and naked-eye detection of hydroxide ion, Sens. Actuators B Chem. 245 (2017) 263–272.
[29] R. Mamgain, F.V. Singh, Selenium-based fluorescence probes for the detection of bioactive molecules, ACS Org. Inorg. Au 2 (2022) 262–288, https://doi.org/10.1021/acsorginorgau.1c00047.
[30] J. Zhang, et al., Pyridinium substituted BODIPY as NIR fluorescent probe for simultaneous sensing of hydrogen sulphide/glutathione and cysteine/homocysteine, Sens. Actuators B Chem. 257 (2018) 1076–1082.
[31] S.T. Manjare, Y. Kim, D.G. Churchill, Selenium- and tellurium-containing fluorescent molecular probes for the detection of biologically important analytes, Acc. Chem. Res. 47 (2014) 2985–2998.
[32] X.H. Xu, C. Liu, Y. Mei, Q.H. Song, BODIPY-based selenides as fluorescent probes for rapid, sensitive and mitochondria-specific detection of hypochlorous acid, J. Mater. Chem. B 7 (2019) 6861–6867.
[33] B.S. Cugnasca, F. Wodtke, A.A. Dos Santos, Seleno-functionalization of BODIPY fluorophores assisted by oxidative nucleophilic hydrogen substitution, Curr. Chem. Biol. 15 (2021) 215–221.
[34] P.P. Deshmukh, A. Navalkar, S.K. Maji, S.T. Manjare, Phenylselenyl containing turn-on dibodipy probe for selective detection of superoxide in mammalian breast cancer cell line, Sens. Actuators B Chem. 281 (2019) 8–13.
[35] S.T. Salunke, D.S. Shelar, S.T. Manjare, Synthesis and photophysical study of tetraphenyl substituted BODIPY Based phenyl-monoselenide probe for selective detection of superoxide, J. Fluoresc. 33 (2023) 437–444.
[36] E. Palao, T. Slanina, P. Klán, Construction of the carbon-chalcogen (S, Se, Te) bond at the 2,6-positions of BODIPY via Stille cross-coupling reaction, Chem. Commun. 52 (2016) 11951–11954.
[37] B. Wang, F. Yu, P. Li, X. Sun, K. Han, A BODIPY fluorescence probe modulated by selenoxide spirocyclization reaction for peroxynitrite detection and imaging in living cells, Dyes Pigm. 96 (2013) 383–390.
[38] S.V. Mulay, et al., Enhanced fluorescence turn-on imaging of hypochlorous acid in living immune and cancer cells, Chem. A Eur. J. 22 (2016) 9642–9648.
[39] S. Fery-Forgues, D. Lavabre, Are fluorescence quantum yields so tricky to measure? A demonstration using familiar stationery products, J. Chem. Educ. 76 (9) (1999) 1260.
[40] W. Wang, A.D.Q. Li, Design and synthesis of efficient fluorescent dyes for incorporation into DNA backbone and biomolecule detection, Bioconjug. Chem. 18 (2007) 1036–1052.
[41] B.J. Littler, et al., Refined synthesis of 5-substituted dipyrromethanes, J. Org. Chem. 64 (1999) 1391–1396, https://doi.org/10.1021/jo982015.
[42] S. Madhu, R. Gonnade, M. Ravikanth, Synthesis of 3,5-bis(acrylaldehyde) boron-dipyrromethene and application in detection of cysteine and homocysteine in living cells, J. Org. Chem. 78 (2013) 5056–5060.
[43] Y. Kim, et al., Exceptional time response, stability and selectivity in doubly-activated phenyl selenium-based glutathione-selective platform, Chem. Sci. 6 (2015) 5435–5439.
[44] A.C. Gonçalves, J.L. Capelo, C. Lodeiro, A.A.D. Santos, A seleno-pyrene selective probe for Hg^{2+} detection in either aqueous or aprotic systems, Sens. Actuators B Chem. 239 (2017) 311–318.
[45] A.A. Soares-Paulino, et al., Nanomolar detection of palladium (II) through a novel seleno-rhodamine-based fluorescent and colorimetric chemosensor, Dyes Pigm. 179 (2020).
[46] K. Zlatić, et al., Spectroscopic and photophysical properties of mono- and dithiosubstituted BODIPY dyes, J. Photochem. Photobiol. A Chem. 388 (2020).
[47] W. Qin, et al., Synthesis, spectroscopy, crystal structure, electrochemistry, and quantum chemical and molecular dynamics calculations of a 3-anilino difluoroboron dipyrromethene dye, J. Phys. Chem. A 113 (2009) 439–447.
[48] P. Rybczynski, et al., Photochemical properties and stability of bodipy dyes, Int J Mol Sci 22 (2021).

[49] W. Qin, et al., Solvent-dependent photophysical properties of borondipyrromethene dyes in solution, Chem. Phys. Lett. 420 (2006) 562–568.
[50] W. Xie, et al., Recent progress in the rational design of biothiol-responsive fluorescent probes, Molecules 28 (2023), https://doi.org/10.3390/molecules28104252.
[51] A. Loudet, K. Burgess, BODIPY dyes and their derivatives: Syntheses and spectroscopic properties, Chem. Rev. 107 (2007) 4891–4932, https://doi.org/10.1021/cr078381n.
[52] S.V. Mulay, et al., Substituent effects in BODIPY in live cell imaging, Chem. Asian J. 11 (2016) 3598–3605.
[53] T. Yang, J. Fan, Y. He, Y. Han, A selenium-based fluorescent probe for the sensitive detection of hypochlorous acid and its application in cell and zebrafish imaging, J. Photochem. Photobiol. A Chem. 447 (2024).
[54] L.Y. Niu, et al., BODIPY-based fluorescent probe for the simultaneous detection of glutathione and cysteine/homocysteine at different excitation wavelengths, RSC Adv. 5 (2015) 3959–3964.
[55] M. Deiana, et al., Site-selected thionated benzothioxanthene chromophores as heavy-atom-free small-molecule photosensitizers for photodynamic therapy, Commun. Chem. 5 (2022).
[56] J.T. Hou, et al., Fluorescent detectors for hydroxyl radical and their applications in bioimaging: A review, Coord. Chem. Rev. 421 (2020), https://doi.org/10.1016/j.ccr.2020.213457.